Electronic Supplementary Material (ESI) for Nanoscale.


**Electronic Supplementary Information for the article:**

# Directional effects in plasmon excitation and transition radiation from an anisotropic 2D material induced by a fast charged particle

Kamran Akbari*,† and Zoran L. Mišković*,†,‡

†*Department of Applied Mathematics, University of Waterloo, Waterloo, Ontario, Canada*

‡*Waterloo Institute for Nanotechnology, University of Waterloo, Waterloo, Ontario, Canada*

E-mail: kamran.a1277@gmail.com; zmiskovi@uwaterloo.ca

In this Supporting Information, we provide details for the theory outlined in the Main Text (MT) and show additional results, which complement and expand upon those discussed in the MT.

# Theory

## Electric dyadic Green's function

Performing a 2D spatial Fourier transform ($\mathbf{r} = \{x, y\} \rightarrow \mathbf{k} = \{k_x, k_y\}$), and a Fourier transform with respect to time ($t \rightarrow \omega$), enables us to express the electric field $\mathbf{E}$ (and other functions of $\mathbf{R} = \{\mathbf{r}, z\}$ and $t$) as

$$\mathbf{E}(\mathbf{R}, t) = \iint \frac{d^2\mathbf{k}}{(2\pi)^2} \mathrm{e}^{i\mathbf{k}\cdot\mathbf{r}} \int_{-\infty}^{\infty} \frac{d\omega}{2\pi} \mathrm{e}^{-i\omega t} \mathbf{E}(\mathbf{k}, z, \omega). \tag{S1}$$

In order to evaluate the electromagnetic (EM) fields, it is convenient to introduce dyadic Green's function (DGF) of the first kind,[1] which may be derived by considering the electric Hertz vector $\mathbf{\Pi}(\mathbf{R}, t)$.[2] Thus, using the relation between the electric field and the Hertz vector,[1,2] one can obtain the EDGF via[1]

$$\overleftrightarrow{G}_{e0}(\mathbf{k}, z, \omega) = \left( k_d^2 \overleftrightarrow{I} - \mathbf{k}\mathbf{k} + i\frac{\partial}{\partial z} (\mathbf{k}\hat{\mathbf{z}} + \hat{\mathbf{z}}\mathbf{k}) + \frac{\partial^2}{\partial z^2} \hat{\mathbf{z}}\hat{\mathbf{z}} \right) G_{\Pi 0}(\mathbf{k}, z, \omega). \tag{S2}$$

where $\overleftrightarrow{I}$ is a 3D identity tensor and $G_{\Pi 0}(\mathbf{k}, z, \omega)$ is the retarded scalar Green's function (GF) for the components of the Hertz vector. This GF is a solution to the nonhomogeneous Helmholtz equation with a scalar electric dipole as the source term,[3] which is easily obtained for the proposed geometry of the problem as

$$\left( \frac{\partial^2}{\partial z^2} - q^2 \right) G_{\Pi 0}(\mathbf{k}, z, \omega) = -\frac{4\pi i}{\omega \epsilon_d(\omega)} \delta(z), \tag{S3}$$

where $k = \sqrt{k_x^2 + k_y^2}$, $q^2 = k^2 - k_d^2$ with $k_d^2 = \omega^2 \epsilon_d(\omega)/c^2$, and is given by

$$G_{\Pi 0}(k, z, \omega) = \frac{2\pi i}{\omega q \epsilon_d(\omega)} \mathrm{e}^{-q|z|}, \tag{S4}$$

with $q(k, \omega)$ specified in Eq. (7) of the MT.

Finally, using Eq. (S4), one may expand the expression in Eq. (S2) to give the full EDGF as

$$\overleftrightarrow{G}_{e0}(\mathbf{k},z,\omega) = \overleftrightarrow{G}^{||}_{e0}(\mathbf{k},z,\omega) - \frac{2\pi i}{\omega q \epsilon_d}\left\{iq\left[k_x\left(\hat{\mathbf{x}}\hat{\mathbf{z}}+\hat{\mathbf{z}}\hat{\mathbf{x}}\right)+k_y\left(\hat{\mathbf{y}}\hat{\mathbf{z}}+\hat{\mathbf{z}}\hat{\mathbf{y}}\right)\right]\mathrm{sign}(z) - \left[k^2-2q\delta(z)\right]\hat{\mathbf{z}}\hat{\mathbf{z}}\right\}\mathrm{e}^{-q|z|}, \tag{S5}$$

where the part of the EDGF, $\overleftrightarrow{G}^{||}_{e0}(\mathbf{k},z,\omega)$, which only involves components parallel to the conducting sheet is given in Eq. (6) of the MT, with $\hat{\mathbf{x}}$, $\hat{\mathbf{y}}$ and $\hat{\mathbf{z}}$ being unit vectors along the corresponding Cartesian axes.

## Self-consistent solution for the induced electromagnetic fields

Having obtained the EDGF in Eq. (S5), one may, straightforwardly, calculate the external and induced electric fields by inserting the corresponding charge current densities $\mathbf{J}_{\mathrm{ext}}(\mathbf{k},z',\omega)$ and $\mathbf{J}_{\mathrm{ind}}(\mathbf{k},z',\omega)$ in Eq. (1) of the MT. Hence, the external electric field may be written as

$$\mathbf{E}_{\mathrm{ext}}(\mathbf{k},z,\omega) = \mathcal{A}\left(\widetilde{E}_{\mathrm{ext},x}\hat{\mathbf{x}}+\widetilde{E}_{\mathrm{ext},y}\hat{\mathbf{y}}+\widetilde{E}_{\mathrm{ext},z}\hat{\mathbf{z}}\right)\mathrm{e}^{iQz}, \tag{S6}$$

with its amplitude $\mathcal{A}$ defined in Eq. (2) of the MT and $Q=\left(\omega-\mathbf{k}\cdot\mathbf{v}_{||}\right)/v_z$, while its dimensionless Cartesian components are given by

$$\begin{aligned}
\widetilde{E}_{\mathrm{ext},x} &= \frac{1}{\omega k}\left(k_d^2 v_x - k_x\omega\right), \\
\widetilde{E}_{\mathrm{ext},y} &= \frac{1}{\omega k}\left(k_d^2 v_y - k_y\omega\right), \\
\widetilde{E}_{\mathrm{ext},z} &= \frac{1}{\omega k}\left[\left(k_d^2-Q^2\right)v_z - Q\mathbf{k}\cdot\mathbf{v}_{||}\right].
\end{aligned} \tag{S7}$$

Furthermore, one can use the above equations to write the external in-plane electric field as $\mathbf{E}_{\mathrm{ext}||}(\mathbf{k},0,\omega)=\mathcal{A}\left(\widetilde{E}_{\mathrm{ext},x}\hat{\mathbf{x}}+\widetilde{E}_{\mathrm{ext},y}\hat{\mathbf{y}}\right)$ to express the total in-plane electric field on the conduct-

ing sheet from Eq. (4) of the MT as

$$\mathbf{E}_{||}(\mathbf{k},0,\omega) = \overleftrightarrow{\epsilon}^{-1} \cdot \mathbf{E}_{\mathrm{ext}||}(\mathbf{k},0,\omega) \equiv \mathcal{A}\,\widetilde{\mathbf{E}}_0, \tag{S8}$$

where we have factored out the amplitude $\mathcal{A}$ and defined the dimensionless total in-plane electric field,

$$\widetilde{\mathbf{E}}_0 \equiv \widetilde{E}_{0x}\hat{\mathbf{x}} + \widetilde{E}_{0y}\hat{\mathbf{y}}, \tag{S9}$$

with its Cartesian components given by

$$\begin{aligned}
\widetilde{E}_{0x} &= \frac{1}{\Delta k\omega}\left[\left(1 - \hat{\mathbf{y}}\cdot\overleftrightarrow{G}^{||}_{e0}(\mathbf{k},0,\omega)\cdot\overleftrightarrow{\sigma}\cdot\hat{\mathbf{y}}\right)\widetilde{E}_{\mathrm{ext},x} + \left(\hat{\mathbf{x}}\cdot\overleftrightarrow{G}^{||}_{e0}(\mathbf{k},0,\omega)\cdot\overleftrightarrow{\sigma}\cdot\hat{\mathbf{y}}\right)\widetilde{E}_{\mathrm{ext},y}\right], \\
\widetilde{E}_{0y} &= \frac{1}{\Delta k\omega}\left[\left(1 - \hat{\mathbf{x}}\cdot\overleftrightarrow{G}^{||}_{e0}(\mathbf{k},0,\omega)\cdot\overleftrightarrow{\sigma}\cdot\hat{\mathbf{x}}\right)\widetilde{E}_{\mathrm{ext},y} + \left(\hat{\mathbf{y}}\cdot\overleftrightarrow{G}^{||}_{e0}(\mathbf{k},0,\omega)\cdot\overleftrightarrow{\sigma}\cdot\hat{\mathbf{x}}\right)\widetilde{E}_{\mathrm{ext},x}\right].
\end{aligned} \tag{S10}$$

Similarly, one may decompose the induced electric field into Cartesian components by factoring out the amplitude $\mathcal{A}$ and its exponential dependence on $z$. Thus, from Eq. (3) of the MT, one finds

$$\mathbf{E}_{\mathrm{ind}}(\mathbf{k},z,\omega) = \mathcal{A}\left(\widetilde{E}_{\mathrm{ind},x}\hat{\mathbf{x}} + \widetilde{E}_{\mathrm{ind},y}\hat{\mathbf{y}} + \mathrm{sign}(z)\,\widetilde{E}_{\mathrm{ind},z}\hat{\mathbf{z}}\right)\mathrm{e}^{-q|z|}, \tag{S11}$$

where

$$\begin{aligned}
\widetilde{E}_{\mathrm{ind},x} &= \hat{\mathbf{x}}\cdot\overleftrightarrow{G}^{||}_{e0}(\mathbf{k},0,\omega)\cdot\overleftrightarrow{\sigma}\cdot\widetilde{\mathbf{E}}_0, \\
\widetilde{E}_{\mathrm{ind},y} &= \hat{\mathbf{y}}\cdot\overleftrightarrow{G}^{||}_{e0}(\mathbf{k},0,\omega)\cdot\overleftrightarrow{\sigma}\cdot\widetilde{\mathbf{E}}_0, \\
\widetilde{E}_{\mathrm{ind},z} &= \frac{2\pi}{\omega\epsilon_d}\left(\mathbf{k}\cdot\overleftrightarrow{\sigma}\cdot\widetilde{\mathbf{E}}_0\right).
\end{aligned} \tag{S12}$$

For the induced magnetic field, we obtain

$$\begin{aligned}\mathbf{B}_{\mathrm{ind}}(\mathbf{k},z,\omega) &= \frac{c}{i\omega}\left(i\mathbf{k}+\frac{\partial}{\partial z}\hat{\mathbf{z}}\right)\times\mathbf{E}_{\mathrm{ind}}(\mathbf{k},z,\omega)\\ &\equiv \mathcal{A}\left(\mathrm{sign}(z)\,\widetilde{B}_{\mathrm{ind},x}\hat{\mathbf{x}}+\mathrm{sign}(z)\,\widetilde{B}_{\mathrm{ind},y}\hat{\mathbf{y}}+\widetilde{B}_{\mathrm{ind},z}\hat{\mathbf{z}}\right)\mathrm{e}^{-q|z|},\end{aligned} \tag{S13}$$

where

$$\begin{aligned}\widetilde{B}_{\mathrm{ind},x} &= \left[\frac{2\pi k_y}{ck_d^2}\,\mathbf{k}+\frac{cq}{i\omega}\,\hat{\mathbf{y}}\cdot\overleftrightarrow{G}^{\parallel}_{e0}(\mathbf{k},0,\omega)\right]\cdot\overleftrightarrow{\sigma}\cdot\widetilde{\mathbf{E}}_0,\\ \widetilde{B}_{\mathrm{ind},y} &= -\left[\frac{2\pi k_x}{ck_d^2}\,\mathbf{k}+\frac{cq}{i\omega}\,\hat{\mathbf{x}}\cdot\overleftrightarrow{G}^{\parallel}_{e0}(\mathbf{k},0,\omega)\right]\cdot\overleftrightarrow{\sigma}\cdot\widetilde{\mathbf{E}}_0,\\ \widetilde{B}_{\mathrm{ind},z} &= \frac{c}{\omega}\,(k_x\hat{\mathbf{y}}-k_y\hat{\mathbf{x}})\cdot\overleftrightarrow{G}^{\parallel}_{e0}(\mathbf{k},0,\omega)\cdot\overleftrightarrow{\sigma}\cdot\widetilde{\mathbf{E}}_0.\end{aligned} \tag{S14}$$

Finally, the joint probability density for the radiative energy loss in the upper/lower half-space can be obtained from the $z$ component of the real part of the Poynting vector,

$$\begin{aligned}\Re\left\{\hat{\mathbf{z}}\cdot\boldsymbol{\mathcal{P}}(\mathbf{k},z,\omega)\right\} &= \frac{c\,|\mathcal{A}|^2}{4\pi}\,\mathrm{sign}(z)\,\left[\widetilde{E}_{\mathrm{ind},x}\widetilde{B}^{*}_{\mathrm{ind},y}-\widetilde{E}_{\mathrm{ind},y}\widetilde{B}^{*}_{\mathrm{ind},x}\right]\\ &= -\frac{|\mathcal{A}|^2}{2}\frac{\kappa^2}{k_d^2}\,G_{\Pi 0}(k,0,\omega)\,\mathrm{sign}(z)\,\left|\mathbf{k}\cdot\overleftrightarrow{\sigma}\cdot\widetilde{\mathbf{E}}_0\right|^2,\end{aligned} \tag{S15}$$

which is nonzero only inside the light cone. One should note that the above expression may also be written in terms of the in-plane EDGF, as seen in Eq. (S18) below.

## Energy loss probability densities

Considering the Physical definition of each contribution and following the formalism presented in Ref.,[3] we first obtain the total energy loss of the external charged particle due to the work done by the induced field on that particle,

$$F_{\mathrm{ext}}\,(\mathbf{k},\omega) = \frac{1}{4\pi^3\omega}\Re\left\{\mathbf{E}^{H}_{\mathrm{ext}\parallel}(\mathbf{k},0,\omega)\cdot\overleftrightarrow{\sigma}(\mathbf{k},\omega)\cdot\overleftrightarrow{\epsilon}^{-1}(\mathbf{k},\omega)\cdot\mathbf{E}_{\mathrm{ext}\parallel}(\mathbf{k},0,\omega)\right\}, \tag{S16}$$

where the superscript $H$ indicates the Hermitian transform (conjugate transpose) of a tensor. Recalling Eq. (7) of the MT, one notices that the total energy loss density of the external particle $F_{\rm ext}$ may be decomposed into two contributions, $F_{\rm ext}^{<}$ and $F_{\rm ext}^{>}$, coming from different regions of the $(\mathbf{k},\omega)$ space, both inside the light cone, $k<k_d$, and outside the light cone, $k>k_d$, respectively.

On the other hand, as a result of the work done by the total electric field acting on the induced current density in the conducting sheet, one may evaluate the joint probability density for the Ohmic energy loss as

$$F_{\rm Ohm}\left(\mathbf{k},\omega\right)=\frac{1}{4\pi^3\omega}\Re\left\{\mathbf{E}_{\rm ext\|}^{H}(\mathbf{k},0,\omega)\cdot\left(\overleftrightarrow{\epsilon}^{-1}\right)^{H}\cdot\overleftrightarrow{\sigma}\cdot\overleftrightarrow{\epsilon}^{-1}\cdot\mathbf{E}_{\rm ext\|}(\mathbf{k},0,\omega)\right\}. \tag{S17}$$

We note that the Ohmic energy loss density $F_{\rm Ohm}$ may also be decomposed into two contributions, $F_{\rm Ohm}^{<}$ and $F_{\rm Ohm}^{>}$, coming from the regions inside and outside the light cone, respectively. Finally, the joint probability density for the radiative energy loss, which only arises in the region of the $(\mathbf{k},\omega)$ space inside the light cone, is obtained from the flux of the Poynting vector in the far field regions above and below the conducting sheet as

$$F_{\rm rad}(\mathbf{k},\omega)=\frac{-1}{4\pi^3\omega}\left\{\mathbf{E}_{\rm ext\|}^{H}(\mathbf{k},0,\omega)\cdot\left(\overleftrightarrow{\epsilon}^{-1}\right)^{H}\cdot\overleftrightarrow{\sigma}^{H}\cdot\overleftrightarrow{G}_{e0}^{\|}(\mathbf{k},0,\omega)\cdot\overleftrightarrow{\sigma}\cdot\overleftrightarrow{\epsilon}^{-1}\cdot\mathbf{E}_{\rm ext\|}(\mathbf{k},0,\omega)\right\}. \tag{S18}$$

To simplify the notation in Eqs. (S17) and (S18), we have dropped the variables $(\mathbf{k},\omega)$ in the tensors $\overleftrightarrow{\sigma}$ and $\overleftrightarrow{\epsilon}$, but we kept them in the electric field components. Referring to Eqs. (6) and (7) of the MT, one should note that inside the light cone and for a lossless surrounding dielectric, $\overleftrightarrow{G}_{e0}^{\|}(\mathbf{k},0,\omega)$ appearing in Eq. (S18) is a purely real-valued symmetric tensor.

When the in-plane conductivity of an anisotropic sheet is considered in the local limit ($k\to 0$), then its tensor may be diagonalized in the Cartesian coordinates, giving

$$\overleftrightarrow{\sigma}(\omega)=\sigma_x(\omega)\,\hat{\mathbf{x}}\hat{\mathbf{x}}+\sigma_y(\omega)\,\hat{\mathbf{y}}\hat{\mathbf{y}}. \tag{S19}$$

Then, also, the effective 2D dielectric tensor of the sheet, defined in Eq. (5) of the MT, takes a simpler form. As a result, one can further streamline the expressions for the energy loss probability densities, given in Eqs. (S16), (S17) and (S18), into

$$F_{\text{ext}}\left(\mathbf{k},\omega\right)=\frac{\left|\mathcal{A}\right|^{2}}{4\pi^{3}\omega}\,\left[\widetilde{E}_{\text{ext},x}\Re\left\{\sigma_{x}\,\widetilde{E}_{0x}\right\}+\widetilde{E}_{\text{ext},y}\Re\left\{\sigma_{y}\,\widetilde{E}_{0y}\right\}\right], \tag{S20}$$

$$F_{\text{Ohm}}\left(\mathbf{k},\omega\right)=\frac{\left|\mathcal{A}\right|^{2}}{4\pi^{3}\omega}\,\left[\left|\widetilde{E}_{0x}\right|^{2}\Re\left\{\sigma_{x}\right\}+\left|\widetilde{E}_{0y}\right|^{2}\Re\left\{\sigma_{y}\right\}\right], \tag{S21}$$

and

$$F_{\text{rad}}(\mathbf{k},\omega)=\frac{\left|\mathcal{A}\right|^{2}}{4\pi^{3}\omega}\frac{2\pi}{\omega\kappa\epsilon_{d}}\,\left[\left(k_{d}^{2}-k_{x}^{2}\right)\left|\sigma_{x}\,\widetilde{E}_{0x}\right|^{2}+\left(k_{d}^{2}-k_{y}^{2}\right)\left|\sigma_{y}\,\widetilde{E}_{0y}\right|^{2}-2k_{x}k_{y}\Re\left\{\sigma_{x}\,\widetilde{E}_{0x}\,\sigma_{y}^{*}\,\widetilde{E}_{0y}^{*}\right\}\right], \tag{S22}$$

respectively. In the above expressions, the dimensionless components of the total in-plane electric field, which are defined in Eq. (S10), may also be written in a simpler form for the case of diagonal conductivity tensor in Eq. (S19), as follows

$$\begin{aligned}\widetilde{E}_{0x}&=\frac{1}{\Delta}\left\{\widetilde{E}_{\text{ext},x}-\frac{2\pi i}{qkc^{2}}\,\sigma_{y}\left[\left(k_{d}^{2}-k_{y}^{2}\right)v_{x}+k_{x}\left(k_{y}v_{y}-\omega\right)\right]\right\},\\ \widetilde{E}_{0y}&=\frac{1}{\Delta}\left\{\widetilde{E}_{\text{ext},y}-\frac{2\pi i}{qkc^{2}}\,\sigma_{x}\left[\left(k_{d}^{2}-k_{x}^{2}\right)v_{y}+k_{y}\left(k_{x}v_{x}-\omega\right)\right]\right\}.\end{aligned} \tag{S23}$$

with $\widetilde{E}_{\text{ext},x}$ and $\widetilde{E}_{\text{ext},y}$ given in Eq. (S7) and $\Delta$ given in Eq. (11) of the MT.

In the MT, we have used $F_{\text{Ohm}}(\mathbf{k},\omega)$ to define the momentum-integrated and the frequency-integrated marginal probability densities $P(\omega)$ and $\Gamma(\mathbf{k})$, respectively. While the latter function provides insight into the direction of excited plasmon polariton modes in phosphorene, it combines contributions from elliptic and hyperbolic dispersion regimes. Therefore, it is worthwhile defining yet another marginal density function, $\Upsilon(\phi,\omega)$, which is obtained by switching wavevector to polar

coordinates, $\mathbf{k} = k(\cos\phi, \sin\phi)$, and integrating over its magnitude $k = \|\mathbf{k}\|$, as follows,

$$\Upsilon(\phi, \omega) = \int_0^\infty dk\, k\, F_{\rm Ohm}\left(k, \phi, \omega\right). \tag{S24}$$

This function is particularly suitable in representing the anisotropy in exciting hyperbolic modes, because its angular dependence should peak at the directions of their asymptotes for (reduced) frequencies $\overline{\omega} > \overline{\omega}_t = 0.69$. Obviously, $P(\omega) = \int_0^{2\pi} d\phi\, \Upsilon(\phi, \omega)$.

Finally, we comment on the expected directionality in exciting plasmon polariton modes in phosphorene, which is expected to be pronounced for grazing incidence of the external charged particle. One can see in Eqs. (S20), (S21) and (S22), that the all joint probability densities are proportional to the factor $|\mathcal{A}|^2$, which enforces the kinematic resonance condition, $\omega = \mathbf{k} \cdot \mathbf{v}_\parallel$, in the limit of an extremely oblique incidence, or near-parallel incidence of the charged particle, where $\theta_0 \to \frac{\pi}{2}$, i.e., $v_z \ll \|\mathbf{v}_\parallel\|$. Assuming that $v < c/\sqrt{\epsilon_d}$, one can then show that

$$|\mathcal{A}|^2 \to 16\pi^3 \frac{(Ze)^2 k^2}{v_z \alpha^3}\, \delta\big(\omega - \mathbf{k} \cdot \mathbf{v}_\parallel\big)\,, \tag{S25}$$

where the delta function expresses the kinematic resonance condition, $\omega = \mathbf{k} \cdot \mathbf{v}_\parallel$, which automatically places the relevant regions of the $(\mathbf{k}, \omega)$ space outside the light cone, hence justifying the choice $q = \alpha$. Accordingly, the TR from the sheet is heavily suppressed for near-parallel incidence.[4,5] Of course, the directional effects from the particle's trajectory also come from the velocity components $v_x$ and $v_y$ in the factors $\widetilde{E}_{0x}$ and $\widetilde{E}_{0y}$, defined in Eq. (S23) with Eq. (S7).

## Modal decomposition of plasmon excitations

Using matrix representation, $\underline{\underline{\epsilon}}$, for the effective 2D dielectric function of an anisotropic sheet, given in Eq. (5) of the MT, in the case when its in-plane conductivity is considered in the local limit, Eq. (S19), we can solve the corresponding eigenvalue problem $\underline{\underline{\epsilon}}\, \underline{\mathbf{u}}_\mp = \lambda_\mp\, \underline{\mathbf{u}}_\mp$. This enables

us to express the function in Eq. (11) of the MT as $\Delta = \lambda_- \lambda_+$, where

$$\lambda_{\mp}(\mathbf{k},\omega) = 1 + 2\pi i \frac{q}{\omega}\left(\sigma_m \mp \sqrt{\sigma_d^2 + \sigma_{\rm int}^2}\right), \tag{S26}$$

with

$$\sigma_{m,d} = \frac{1}{2q^2}\left[\left(k_y^2 - k_d^2\right)\,\sigma_y(\omega) \pm \left(k_x^2 - k_d^2\right)\,\sigma_x(\omega)\right], \tag{S27}$$

and $\sigma_{\rm int} = \frac{k_x k_y}{q^2}\sqrt{\sigma_x(\omega)\sigma_y(\omega)}$. One may compare this equation with Eq. (14) in Ref.[6] describing hybridization of plasmon polaritons in double-layer graphene. Therefore, solving the equation $\Delta(\mathbf{k},\omega) = 0$ in the limit of vanishing real parts of the conductivity tensor components is naturally decomposed into two equations, $\lambda_-(\mathbf{k},\omega) = 0$ and $\lambda_+(\mathbf{k},\omega) = 0$, giving the dispersion relations of two eigen-modes, $\omega = \omega_-(\mathbf{k})$ and $\omega = \omega_+(\mathbf{k})$, respectively. Those eigenfrequencies represent longitudinal and transverse modes, which are hybridized when they propagate with the wavevector $\mathbf{k} = (k,\theta)$ at an arbitrary angle $\theta$ with respect to the principal axes of phosphorene.[7]

The eigenvectors corresponding to the eigenvalues $\lambda_{\mp}$, given in Eq. (S26), may be written as

$$\underline{\mathbf{u}}_{\mp} = N_{\mp}\begin{bmatrix} \frac{k_x k_y}{\alpha^2}\sigma_y \\ \sigma_d \mp \sqrt{\sigma_d^2 + \sigma_{\rm int}^2} \end{bmatrix}, \tag{S28}$$

where $N_{\mp}$ are normalization factors. Using eigenvalue decomposition, we may write the matrix representation of the 2D dielectric tensor as $\underline{\underline{\epsilon}} = \underline{\underline{\mathbf{U}}}\,\underline{\underline{\mathbf{\Lambda}}}\,\underline{\underline{\mathbf{U}}}^{-1}$, where $\underline{\underline{\mathbf{U}}} = \left[\underline{\mathbf{u}}_- \;\; \underline{\mathbf{u}}_+\right]$ and $\underline{\underline{\mathbf{\Lambda}}} = \mathrm{diag}\left[\lambda_- \;\; \lambda_+\right]$. Thus, one may express the tangential components of the total in-plane electric field as a modal decomposition, $\underline{\mathbf{E}}_0 = \underline{\underline{\epsilon}}^{-1}\,\underline{\mathbf{E}}_{\mathrm{ext}||}(\mathbf{k},0,\omega) = \underline{\underline{\mathbf{U}}}\,\underline{\underline{\mathbf{\Lambda}}}^{-1}\,\underline{\underline{\mathbf{U}}}^{-1}\underline{\mathbf{E}}_{\mathrm{ext}||}(\mathbf{k},0,\omega)$. Consequently, each component of the total tangential electric field may be written as

$$\widetilde{E}_{0x,y} = \frac{C_{x,y}^-}{\lambda_-} + \frac{C_{x,y}^+}{\lambda_+}, \tag{S29}$$

where

$$
\begin{aligned}
C_x^{\mp} &= \frac{1}{2}\left[\left(1 \pm \frac{\sigma_d}{\sqrt{\sigma_d^2+\sigma_{\rm int}^2}}\right)\widetilde{E}_{{\rm ext},x} \mp \frac{k_x k_y\,\sigma_y}{\alpha^2\sqrt{\sigma_d^2+\sigma_{\rm int}^2}}\,\widetilde{E}_{{\rm ext},y}\right], \\
C_y^{\mp} &= \frac{1}{2}\left[\mp\frac{k_x k_y\,\sigma_x}{\alpha^2\sqrt{\sigma_d^2+\sigma_{\rm int}^2}}\,\widetilde{E}_{{\rm ext},x} + \left(1 \mp \frac{\sigma_d}{\sqrt{\sigma_d^2+\sigma_{\rm int}^2}}\right)\widetilde{E}_{{\rm ext},y}\right],
\end{aligned}
\tag{S30}
$$

with $\widetilde{E}_{{\rm ext},x}$ and $\widetilde{E}_{{\rm ext},y}$ given in the first two lines of Eq. (S7).

Notice that the singular nature of the terms in Eq. (S29) exposes possibly strong roles of the two eigen-modes when calculating various energy loss channels in the regions of the $(\mathbf{k},\omega)$ space where $\lambda_{\mp}(\mathbf{k},\omega) \to 0$ in the limit of vanishing dissipation in the conducting sheet. Considering that the corresponding dispersion relations, $\omega = \omega_{\mp}(\mathbf{k})$, are located outside the light cone, $k > k_d$, and taking the limit $\Re\{\sigma_x(\omega)\} = \Re\{\sigma_y(\omega)\} \to 0^+$, one expects that the total energy loss outside the light cone is dominated by the Ohmic energy loss that goes entirely to the excitation of the two long-lived eigen-modes, i.e., $F_{\rm ext}^{>}(\mathbf{k},\omega) = F_{\rm Ohm}^{>}(\mathbf{k},\omega) \to F_{\rm pl}(\mathbf{k},\omega)$, where $F_{\rm pl}(\mathbf{k},\omega)$ is defined as the joint probability density for plasmon excitations. Inserting Eq. (S29) into Eq. (S20) then shows that the plasmon excitation probability density may be decomposed into two modal contributions, $F_{\rm pl}(\mathbf{k},\omega) = F_{\rm pl}^{-}(\mathbf{k},\omega) + F_{\rm pl}^{+}(\mathbf{k},\omega)$, which are given by

$$
\begin{aligned}
F_{\rm pl}^{\mp}(\mathbf{k},\omega) &= \frac{|\mathcal{A}|^2}{4\pi^3\omega}\,\Re\left\{\frac{1}{\lambda_{\mp}}\left[\widetilde{E}_{{\rm ext},x}\,\sigma_x(\omega)\,C_x^{\mp} + \widetilde{E}_{{\rm ext},y}\,\sigma_y(\omega)\,C_y^{\mp}\right]\right\}\Bigg|_{\Re\{\sigma_x\}=\Re\{\sigma_y\}\to 0^+} \\
&= \frac{|\mathcal{A}|^2}{4\pi^2\omega}\,\left\{\frac{1}{2}\widetilde{E}_{{\rm ext},x}^2\left[\Im\{\sigma_x\}\left(1 \pm \frac{\Im\{\sigma_d\}}{\mathcal{D}(k_x,k_y)}\right)\right] \mp \frac{k_x k_y}{\alpha^2}\widetilde{E}_{{\rm ext},x}\widetilde{E}_{{\rm ext},y}\left[\frac{\Im\{\sigma_x\}\,\Im\{\sigma_y\}}{\mathcal{D}(k_x,k_y)}\right]\right. \\
&\qquad \left. + \frac{1}{2}\widetilde{E}_{{\rm ext},y}^2\left[\Im\{\sigma_y\}\left(1 \mp \frac{\Im\{\sigma_d\}}{\mathcal{D}(k_x,k_y)}\right)\right]\right\}\,\delta\Big(\Re\left\{\lambda_{\mp}|_{\Re\{\sigma_x\}=\Re\{\sigma_y\}\to 0^+}\right\}\Big).
\end{aligned}
\tag{S31}
$$

Notice that the above expression involves a Dirac delta function peaked at the zeros of the function that gives rise to the corresponding dispersion relation $\omega = \omega_{\mp}(\mathbf{k})$, which may be written in the

limit of vanishing damping in the sheet as

$$\Re\left\{\lambda_{\mp}|_{\Re\{\sigma_x\}=\Re\{\sigma_y\}\to 0^+}\right\} = 1 - \frac{\pi}{\omega\alpha}\left[\left(k_x^2 - k_d^2\right)\Im\left\{\sigma_x\right\} + \left(k_y^2 - k_d^2\right)\Im\left\{\sigma_y\right\} \mp \mathcal{D}(k_x, k_y)\right], \tag{S32}$$

where

$$\mathcal{D}(k_x, k_y) = \sqrt{\left(k_x^2 - k_d^2\right)^2\Im\left\{\sigma_x\right\}^2 + \left(k_y^2 - k_d^2\right)^2\Im\left\{\sigma_y\right\}^2 + 2\left(k_x^2 k_y^2 + \alpha^2 k_d^2\right)\Im\left\{\sigma_x\right\}\Im\left\{\sigma_y\right\}}. \tag{S33}$$

Note that the above result in Eq. (S31) provides a good approximation for Ohmic energy losses outside the light cone in the case of small but finite damping in the conducting sheet, $F_{\mathrm{Ohm}}\left(\mathbf{k},\omega\right) \approx F_{\mathrm{Ohm}}^{>}\left(\mathbf{k},\omega\right) \approx F_{\mathrm{pl}}\left(\mathbf{k},\omega\right)$. More importantly, the singular behavior of the expression in Eq. (S31) at frequencies $\omega = \omega_{\mp}(\mathbf{k})$, when coupled with the expression for $\left|\mathcal{A}\right|^2$ given in Eq. (S25) in the limit of oblique incidence, which involves a delta function $\delta\big(\omega - \mathbf{k}\cdot\mathbf{v}_{\parallel}\big)$, provides a mechanism for exciting the plasmon modes in the conducting sheet by a kinematic resonance condition, $\omega_{\mp}(\mathbf{k}) = \mathbf{k}\cdot\mathbf{v}_{\parallel}$. It is expected that, in the regime of hyperbolic plasmon dispersion in the sheet, a suitable choice of the incident charged particle trajectory may give rise to strong directionality effects in exciting such plasmon modes.

In the case of isotropic conductivity, i.e., when $\sigma_x(\omega) = \sigma_y(\omega) = \sigma_{\mathrm{iso}}(\omega)$, the longitudinal and transverse modes are no longer hybridized. We then have $\Delta = \lambda_t\lambda_l$, with $\lambda_- \to \lambda_t$ and $\lambda_+ \to \lambda_l$, where $\lambda_t = 1 - 2\pi i\frac{\omega}{c^2 q}\sigma_{\mathrm{iso}}(\omega)$ and $\lambda_l = 1 + 2\pi i\frac{q}{\omega}\sigma_{\mathrm{iso}}(\omega)$ correspond to the transverse and longitudinal modes, respectively.

In a high frequency range, which is relevant for the hyperbolic regime, we may can take a nonretarded limit, giving $\Delta \to 1 + 2\pi i\frac{k}{\omega}\sigma_l(\phi,\omega)$, where we define the orientation dependent longitudinal conductivity by $\sigma_l(\phi,\omega) = \cos^2\phi\,\sigma_x(\omega) + \sin^2\phi\,\sigma_y(\omega)$. In this regime, only the longitudinal hyperbolic plasmon mode exists with a particularly simple expression for the excitation

probability density,

$$F_{\rm pl}^{\rm NR}\left(\mathbf{k},\omega\right)=\frac{\left|\mathcal{A}^{\rm NR}\right|^2}{8\pi^3 k}\,\delta\!\left(1-2\pi\frac{k}{\omega}\Im\left\{\sigma_l(\phi,\omega)\right\}\right), \tag{S34}$$

where

$$\mathcal{A}^{\rm NR}=-i4\pi\frac{Ze}{\epsilon_d}\,\frac{kv_z}{k^2v_z^2+\left(\omega-\mathbf{k}\cdot\mathbf{v}_{||}\right)^2}. \tag{S35}$$

# Results

All results in this section will be shown in reduced units using the normalization defined in the MT.

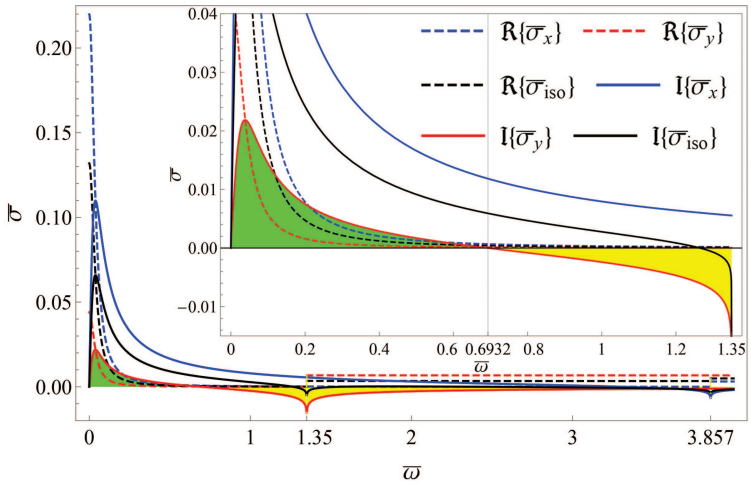


Figure S1: Real and imaginary parts of the normalized conductivity components, $\overline{\sigma}_x=\sigma_x/c$ and $\overline{\sigma}_y=\sigma_y/c$, for the model of anisotropic 2D material given in Eq. (12),[8] shown as a function of the reduced frequency $\overline{\omega}$. Also shown is the normalized conductivity of a hypothetical isotropic material, $\overline{\sigma}_{\rm iso}=\sigma_{\rm iso}/c$.

In Fig. S1, we show the real and imaginary parts of the optical conductivity tensor components for an anisotropic 2D material, Eq. (12) of the MT, evaluated with the parameters given by Nemilentsau *et al.*[8] We shall refer to that material as "phosphorene" in the rest of the text. The vertical bar in the inset at the reduced frequency $\overline{\omega}_t=0.6932$ marks a transition point from the elliptic to the hyperbolic regime of phosphorene, which are indicated by the green and yellow

shading. Also shown in Fig. S1 is the conductivity of a hypothetical isotropic material, defined as $\sigma_{\rm iso}(\omega) = \frac{1}{2}\left[\sigma_x(\omega) + \sigma_y(\omega)\right]$.

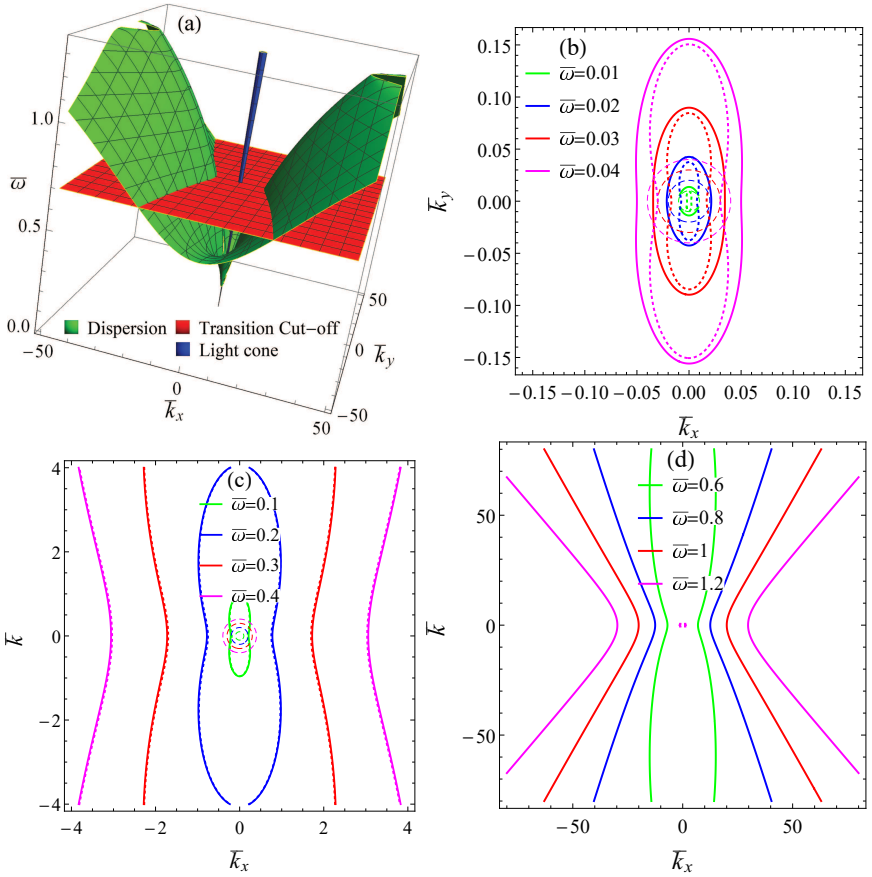


Figure S2: In panel (a), green surface shows the dispersion relation $\overline{\omega} = \overline{\omega}_d(\overline{k}_x, \overline{k}_y)$ for plasmon polaritons, computed from the conductivity model in Eq. (12).[8] Also shown are the light cone $\overline{\omega} = \overline{k}$ (blue) and the plane $\overline{\omega} = 0.69$ (red), which indicates a topological transition where closed iso-frequency curves become open curves. In panels (b), (c) and (d), we show iso-frequency curves for several frequencies in the elliptic, an intermediate, and the hyperbolic regimes, respectively. The solid and dotted lines show fully retarded and non-retarded iso-frequency curves, while the dashed lines are the circles originating from the light cone.

In Fig. S2 we show the dispersion surface in reduced units, $\overline{\omega} = \overline{\omega}_d(\overline{k}_x, \overline{k}_y)$, along with the plane $\overline{\omega} = \overline{\omega}_t$ and the light cone $\overline{\omega} = \sqrt{\overline{k}_x^2 + \overline{k}_y^2}$. One notices that intersections of the dispersion surface with planes of constant $\overline{\omega}$ corresponding to frequencies $\ll 1$ give rise to the iso-frequency curves in the $(\overline{k}_x, \overline{k}_y)$ plane characterized by elliptically shaped closed curves that enclose circles resulting from the corresponding intersections with the light cone. Notice that the close proximity of the elliptic dispersion curves and the light circles implies strong retardation effects on

the plasmon dispersion in the THz frequency range. Accordingly, it is important to use fully retarded calculations in the elliptic regime, i.e., when $\overline{\omega} \ll 1$. We note that the iso-frequency curves get increasingly elongated in the $k_y$ direction (ZZ direction) as the frequency increases, attaining the shape of the numeral 8, while remaining closed curves as long as $\overline{\omega} < \overline{\omega}_t$. The iso-frequency curves become open once the (reduced) frequency exceeds $\overline{\omega}_t$ and they attain the shape of hyperbolas with branches opening along the positive and negative directions of the $k_x$ axis (AC direction). It is permissible to neglect retardation effects in the hyperbolic regime with frequencies $\overline{\omega} \sim 1$.

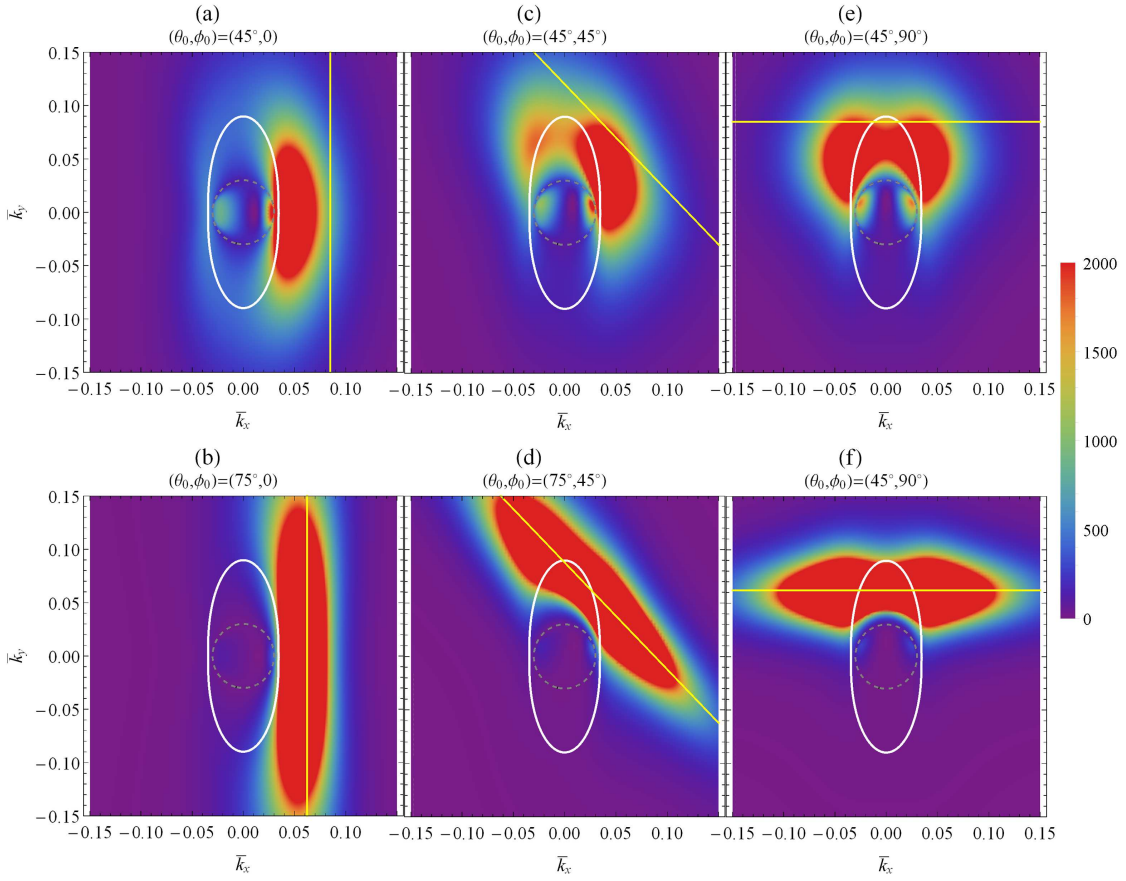


Figure S3: The total energy loss density, $\overline{F}_{\rm ext}(\overline{k}_x, \overline{k}_y, \overline{\omega})$, is shown in the elliptic regime as a function of the reduced wavenumbers $(\overline{k}_x, \overline{k}_y)$ at fixed frequency $\overline{\omega} = 0.03$ for a charged particle at the reduced speed $\beta = 0.5$, with the oblique incidence angles $\theta_0 = 45^\circ$ (a,c,e) and $\theta_0 = 75^\circ$ (b,d,f), in the in-plane directions $\phi_0 = 0$ (a,b), $\phi_0 = 45^\circ$ (c,d) and $\phi_0 = 90^\circ$ (e,f). Also shown are the iso-frequency curve $\bar{\omega}_d(\bar{k}_x, \bar{k}_y) = 0.03$ (white lines), the trace of the light cone (circles with dashed yellow lines) and the straight lines $\bar{k}_x\beta_x + \bar{k}_y\beta_y = 0.03$ (solid yellow lines).

Figures S3 and S4 show the total energy loss density, $\overline{F}_{\rm ext}(\overline{k}_x, \overline{k}_y, \overline{\omega})$, in the elliptic regime (for

a low frequency of $\overline{\omega} = 0.03$ and a fast charged particle with $\beta = 0.5$) and the hyperbolic regime (for a high frequency of $\overline{\omega} = 1$ and a slow charged particle with $\beta = 0.035$), respectively. These figures show the effects of variation in the angles $(\theta_0, \phi_0)$ for obliquely incident particles and, in that way, they complement Fig. 2 in the MT, which discusses normal incidence at both speeds. One can notice that the largest values of $\overline{F}_{\text{ext}}$ outside the light cone occur due to Ohmic losses in the regions of close proximity, or intersection of the corresponding dispersion iso-frequency curves $\bar{\omega}_d(\bar{k}_x, \bar{k}_y) = \bar{\omega}$ and the line $\bar{k}_x\beta_x + \bar{k}_y\beta_y = \overline{\omega}$, where $\beta_x = v_x/c$ and $\beta_y = v_y/c$.

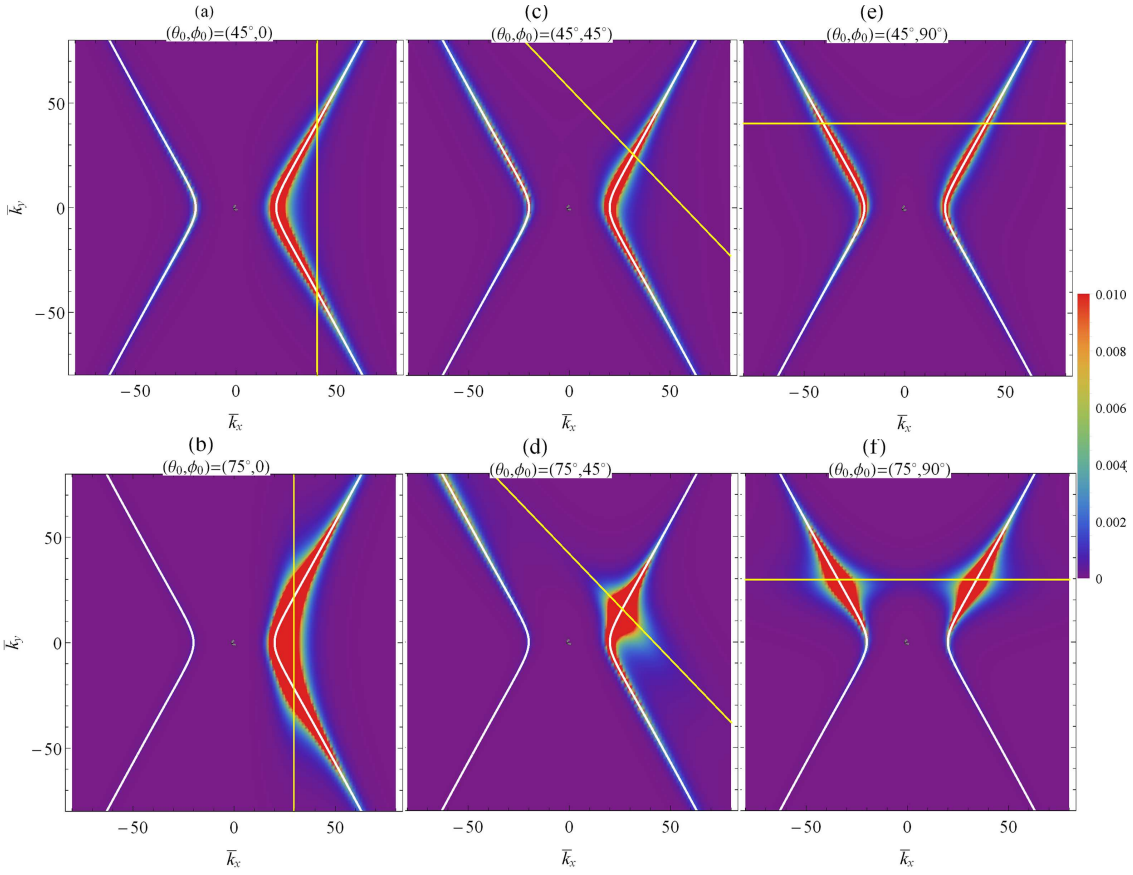


Figure S4: The total energy loss density, $\overline{F}_{\text{ext}}(\overline{k}_x, \overline{k}_y, \overline{\omega})$, is shown in the hyperbolic regime as a function of the reduced wavenumbers $(\overline{k}_x, \overline{k}_y)$ at fixed frequency $\overline{\omega} = 1$ for a charged particle at the reduced speed $\beta = 0.035$, with the oblique incidence angles $\theta_0 = 45°$ (a,c,e) and $\theta_0 = 75°$ (b,d,f), in the in-plane directions with $\phi_0 = 0$ (a,b), $\phi_0 = 45°$ (c,d) and $\phi_0 = 90°$ (e,f). Also shown is the iso-frequency curve $\bar{\omega}_d(\bar{k}_x, \bar{k}_y) = 1$ (white lines), the trace of the light cone (circles with dashed yellow lines) and the straight lines $\bar{k}_x\beta_x + \bar{k}_y\beta_y = 1$ (solid yellow lines).

In Figs. S5, S6, S7 and S8, we show the function $\Upsilon(\phi, \omega)$, defined in Eq. (S24), for normal incidence and oblique incidence of fast ($\beta = 0.5$, upper rows) and slow ($\beta = 0.035$, lower rows)

charged particles. All results in Figs. S5, S6 and S7 are shown for phosphorene (left columns) and are compared to isotropic material (right columns). The horizontal lines at $\overline{\omega}_t = 0.69$ indicate a transition frequency from the elliptic ($\overline{\omega} < \overline{\omega}_t$) to the hyperbolic ($\overline{\omega} > \overline{\omega}_t$) regimes in phosphorene. A comparison between phosphorene and isotropic material for $\beta = 0.5$ in those figures reveals that the distribution $\Upsilon(\phi, \omega)$ has similar shapes at low frequencies, indicating that the Ohmic energy loss due to excitation of the elliptical modes in phosphorene is qualitatively similar to the excitation of modes in an isotropic material by relativistic particles. On the other hand, a comparison for $\beta =$

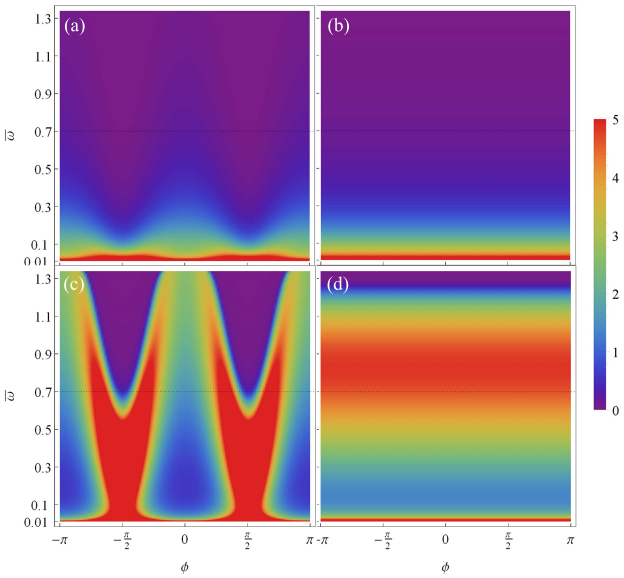


Figure S5: The function $\Upsilon$, defined in Eq. (S24), is shown in reduced units as a function of the reduced frequency $\overline{\omega}$ and polar angle $\phi$ of excited modes for a charged particle under normal incidence at two speeds: $\beta = 0.5$ (a,b) and $\beta = 0.035$ (c,d). Results for phosphorene (a,c) are compared with those for isotropic material (b,d).

$0.035$, shows significant differences between phosphorene and isotropic material. In particular, one notices a strong anisotropy at high frequencies in the former case due to the excitation of hyperbolic modes, which is indicated by a marked depletion in the $\Upsilon(\phi, \omega)$ values at $\phi \approx \pm\frac{\pi}{2}$ for $\overline{\omega} > \overline{\omega}_t$, corresponding to the directions of the mode propagation between two branches of the hyperbolas. At the same time, one also notices a strong anisotropy for $\beta = 0.035$ at low frequencies, pertaining to the excitation of elliptic modes. For the case of normal incidence in Fig. S5, one notices broad peaks in $\Upsilon(\phi, \omega)$ for $\beta = 0.035$ near the angles $\phi = \pm 90°$ at low frequencies, which correspond to the Ohmic energy loss in the ZZ direction, as seen in Fig. 2(b) of the MT in the elliptic regime.

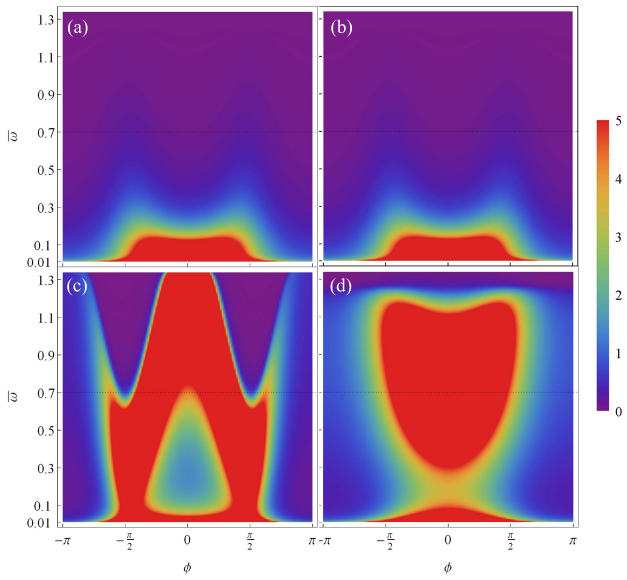


Figure S6: The same as Fig. S5, but for oblique incidence with angles $(\theta_0, \phi_0) = (45°, 0)$.

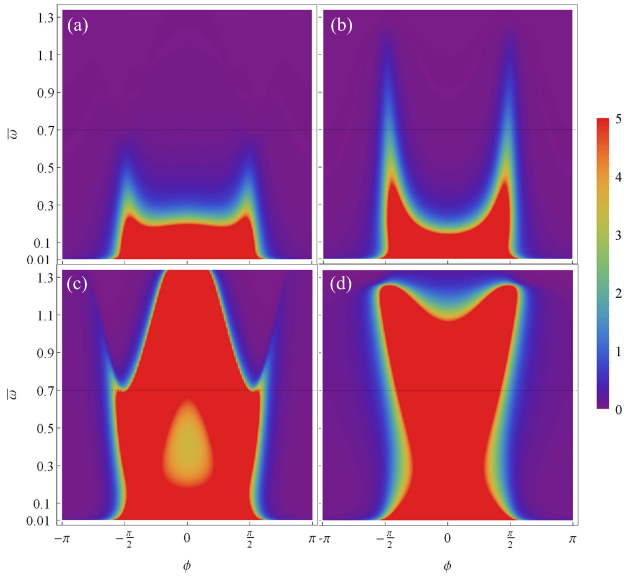


Figure S7: The same as Fig. S5, but for oblique incidence with angles $(\theta_0, \phi_0) = (75°, 0)$.

While in Figs. S6 and S7 the in-plane direction of an obliquely incident particle was $\phi_0 = 0$ (AC direction), in Fig. S8, we show the effects of changing the in-plane direction to $\phi_0 = 45°$ and $\phi_0 = 90°$ (ZZ direction) in the shape of $\Upsilon(\phi, \omega)$ for the same set the oblique angles $\theta_0$ and speeds $\beta$ as in Figs. S6 and S7. In the panels (f) and (h) of Fig. S8, $\Upsilon(\phi, \omega)$ exhibits a strong asymmetry in the hyperbolic regime when the incident particle moves in the $\phi_0 = 90°$ (ZZ) direction at the speed $\beta = 0.035$, with the "V" shaped maxima at $\overline{\omega} > \overline{\omega}_t$ corresponding to the increase in the

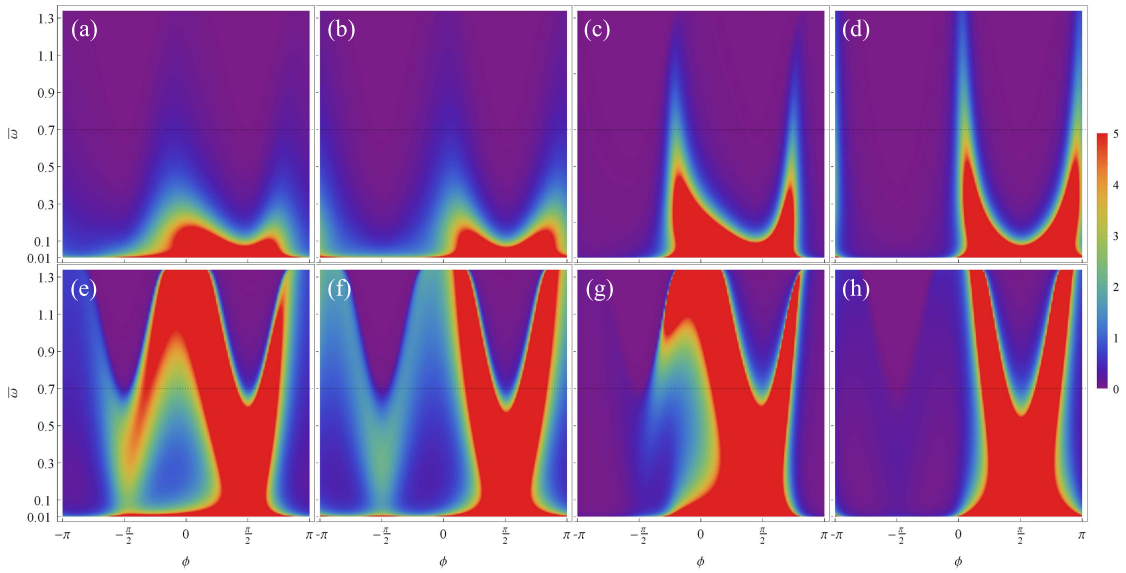


Figure S8: The function $\Upsilon$, defined in Eq. (S24), is shown in reduced units as a function of the reduced frequency $\overline{\omega}$ and polar angle $\phi$ of the excited modes for a charged particle under a generally oblique incidence upon phosphorene at two speeds: $\beta = 0.5$ (a,b,c,d) and $\beta = 0.035$ (e,f,g,h) for the combination of angles: $(\theta_0, \phi_0) = (45°, 45°)$ (a,e), $(\theta_0, \phi_0) = (45°, 90°)$ (b,f), $(\theta_0, \phi_0) = (75°, 45°)$ (c,g) and $(\theta_0, \phi_0) = (75°, 90°)$ (d,h).

opening angles of the asymptotes of corresponding iso-frequency hyperbolas, as seen in the panel (d) of Fig. S2. At the same time, we see in Fig. S8(f,h) for the speed of $\beta = 0.035$ that one of the peaks that occurred for normal incidence in Fig. S5(c) in the directions $\phi = -90°$ in the elliptic regime, is depleted in favor of a broader peak at $\phi = 90°$, which is aligned with the direction of motion of the charged particle in Fig. S8(f,h).

In Fig. S9, we show the frequency-integrated marginal probability density $\Gamma(k_x, k_y)$ for the same set of parameters as in Fig. 3 of the MT, but for a high incident speed of $\beta = 0.5$. As opposed to Fig. 3 of the MT, where a low incident speed of $\beta = 0.035$ was used, we see in Fig. S9 that the main contributions to $\bar{\Gamma}(\bar{k}_x, \bar{k}_y)$ come from the regions $\beta_x \bar{k}_x + \beta_y \bar{k}_y < \bar{\omega}_t$, corresponding to the elliptic regime. While the distributions of $\bar{\Gamma}(\bar{k}_x, \bar{k}_y)$ are still narrow in Fig. S9(i,k,m) for the angle of incidence $\theta_0 = 75°$ upon phosphorene, and they follow the lines $\bar{\omega}_d(\bar{k}_x, \bar{k}_y) = \beta_x \bar{k}_x + \beta_y \bar{k}_y$, we see that those distributions are not very different from the corresponding distributions in the isotropic material in Fig. S9(j,l,n). This is yet another evidence that probing the elliptic regime by relativistic particles in phosphorene is qualitatively similar to that in isotropic materials.

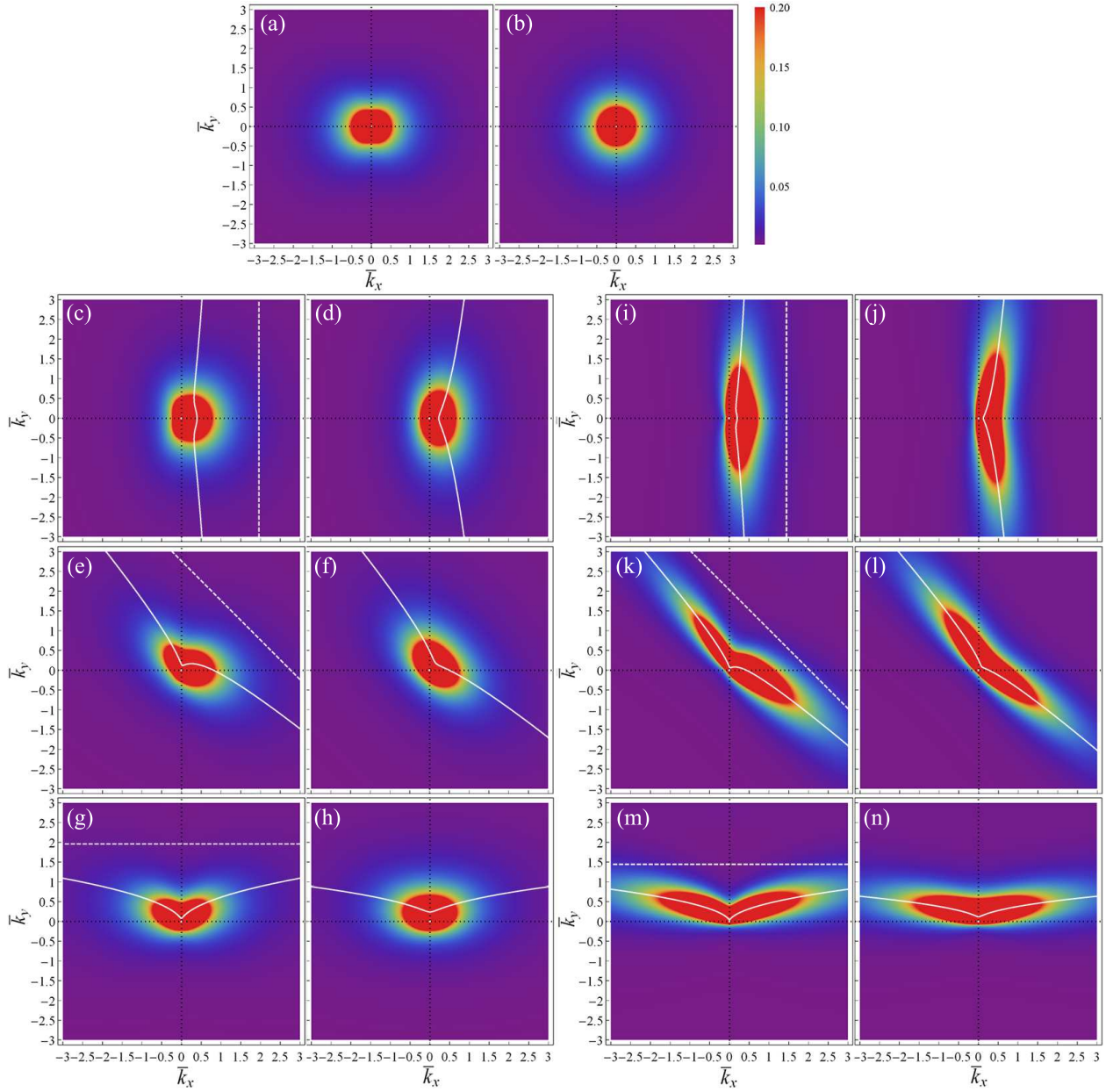


Figure S9: Plots of $\bar{\Gamma}(\bar{k}_x, \bar{k}_y)$ for phosphorene (a,c,e,g,i,k,m) and an isotropic material (b,d,f,h,j,l,n) with the reduced speed $\beta = 0.5$. Besides normal incidence (a,b), the two cases of oblique incidence with $\theta_0 = 45°$ (c,d,e,f,g,h) and $\theta_0 = 75°$ (i,j,k,l,m,n) are shown for the in-plane directions of $\phi_0 = 0$ (c,d,i,j), $\phi_0 = 45°$ (e,f,k,l) and $\phi_0 = 90°$ (g,h,m,n). White solid lines show the curves obtained from the kinematic resonance with plasmon dispersion, $\bar{\omega}_d(\bar{k}_x, \bar{k}_y) = \beta_x \bar{k}_x + \beta_y \bar{k}_y$, whereas the white dashed lines show the line $\beta_x \bar{k}_x + \beta_y \bar{k}_y = \bar{\omega}_t$, with $\bar{\omega}_t \approx 0.69$ indicating a transition from the elliptic to hyperbolic regime in phosphorene.

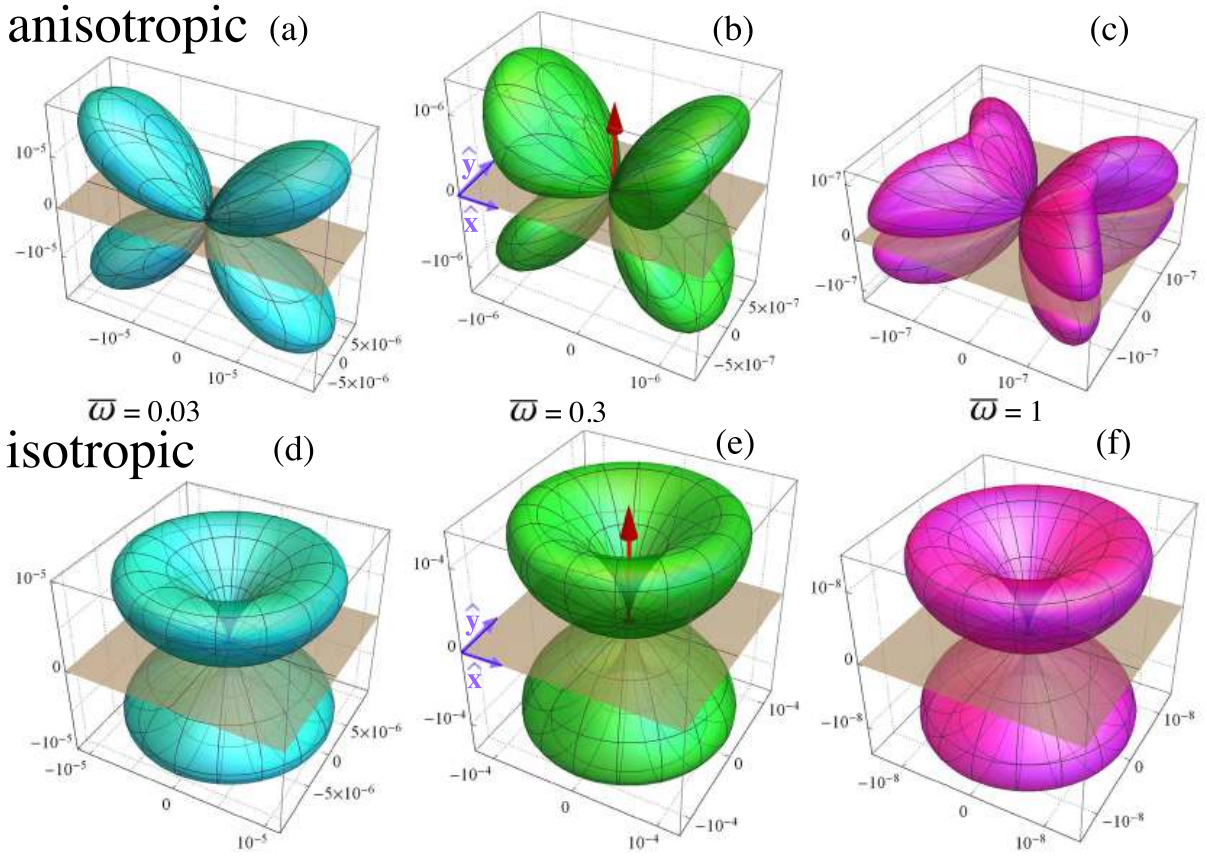


Figure S10: Angular distribution of transition radiation, $\overline{S}(\theta, \phi, \overline{\omega})$, at three reduced frequencies: $\overline{\omega} = 0.03$ (a,d), $\overline{\omega} = 0.3$ (b,e) and $\overline{\omega} = 1$ (c,f) for normal incidence of a charged particle with the reduced speed $\beta = 0.035$ upon: phosphorene (a,b,c) and an isotropic material (d,e,f).

In Fig. S10, we show the spectral angular distribution $\overline{S}(\theta, \phi, \overline{\omega})$ of TR, induced by a normally incident particle moving at the speed $\beta = 0.035$. This figure complements Fig. 5 in the MT, the only difference being that the TR in Fig. S10 is induced by a particle at $\beta = 0.035$, as opposed to $\beta = 0.5$ used in Fig. 5 of the MT. Notwithstanding the substantially smaller magnitudes of $\overline{S}(\theta, \phi, \overline{\omega})$ in Fig. S10, as expected for the TR, it is interesting that the shape of all the spectra are quite similar to the shapes seen in Fig. 5 of the MT, except for phosphorene in the hyperbolic regime in Fig. S10(c). This is perhaps not surprising, given that the excitation of hyperbolic modes in phosphorene is more efficient for slower particles, even though their contribution to radiation energy loss is negligible.

In Figs. S11 and S12, we study the TR spectra for a particle moving at the speed $\beta = 0.5$

with the oblique angle of incidence $\theta_0 = 45°$. In Fig. S11, we compare the spectra of phosphorene emitted when the particle moves in the $\phi_0 = 0$ (AC) direction with the corresponding spectra from isotropic material. One can see that, even though the spectra from isotropic material in Fig. S11(d,e,f) exhibit some asymmetry, as observed before for graphene,[5] phosphorene maintains a strong asymmetry in the spectra in Fig. S11(a,b,c), which is similar to that observed in Fig. 6(a,b,c) of the MT for a larger incidence angle of $\theta_0 = 75°$.

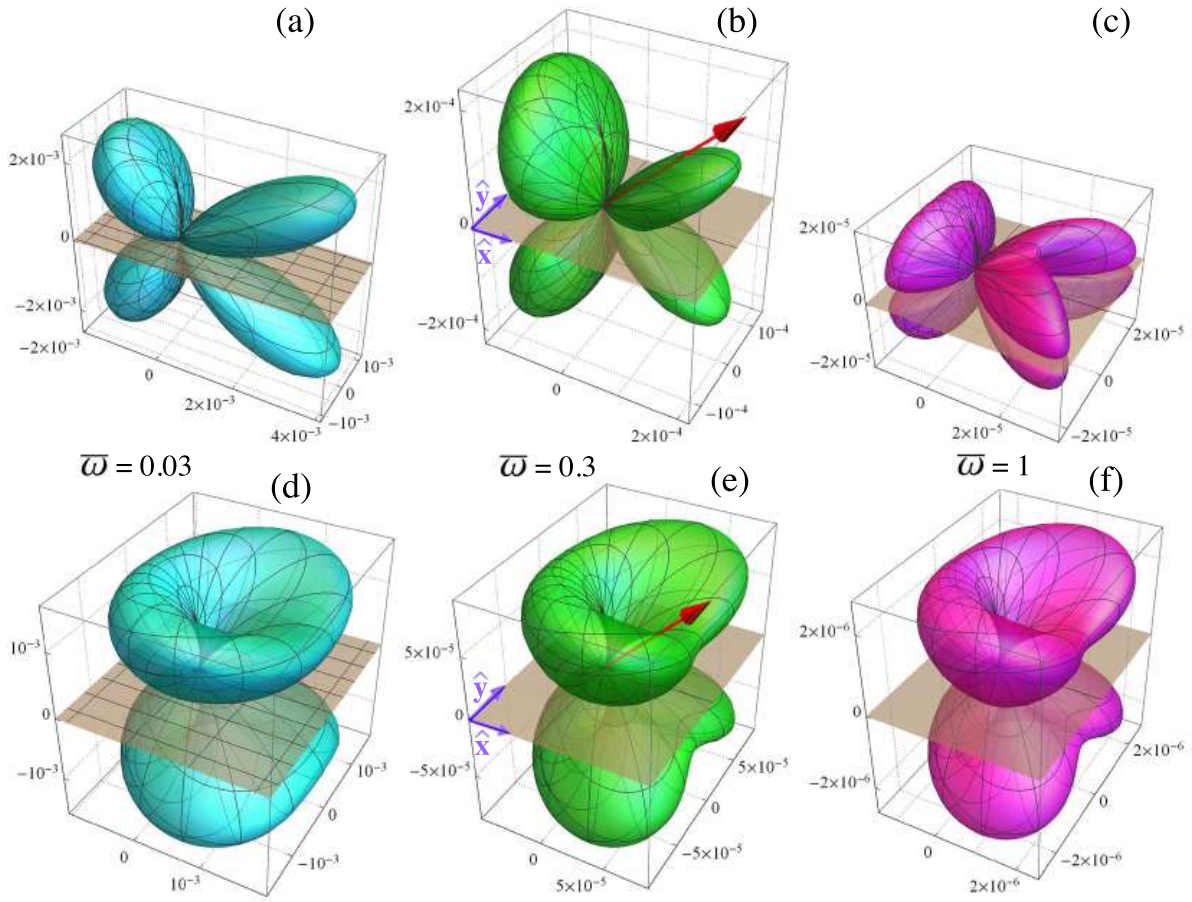


Figure S11: Angular distribution of transition radiation, $\overline{S}(\theta, \phi, \overline{\omega})$, at three reduced frequencies: $\overline{\omega} = 0.03$ (a,d), $\overline{\omega} = 0.3$ (b,e) and $\overline{\omega} = 1$ (c,f) for a charged particle at the reduced speed $\beta = 0.5$, moving under oblique incidence with the angles $(\theta_0, \phi_0) = (45°, 0)$ upon: phosphorene (a,b,c) and an isotropic material (d,e,f).

In Fig. S12, we analyze the effects of changing the in-plane direction to $\phi_0 = 45°$ and $\phi_0 = 90°$ (ZZ direction) for the same oblique angle, $\theta_0 = 45°$, as in Fig. S11. When the particle moves in the ZZ direction, the spectra in Fig. S12(d,e,f) exhibit a similar asymmetry as the spectra in Fig. 6(d,e,f)

of the MT for $\theta_0 = 75°$. Therefore, it appears that the TR spectra do not change much for a fast charged particle as the angle $\theta_0$ of oblique incidence upon phosphorene increases, at least when the particle in-plane directions are oriented along the AC and ZZ symmetry axes.

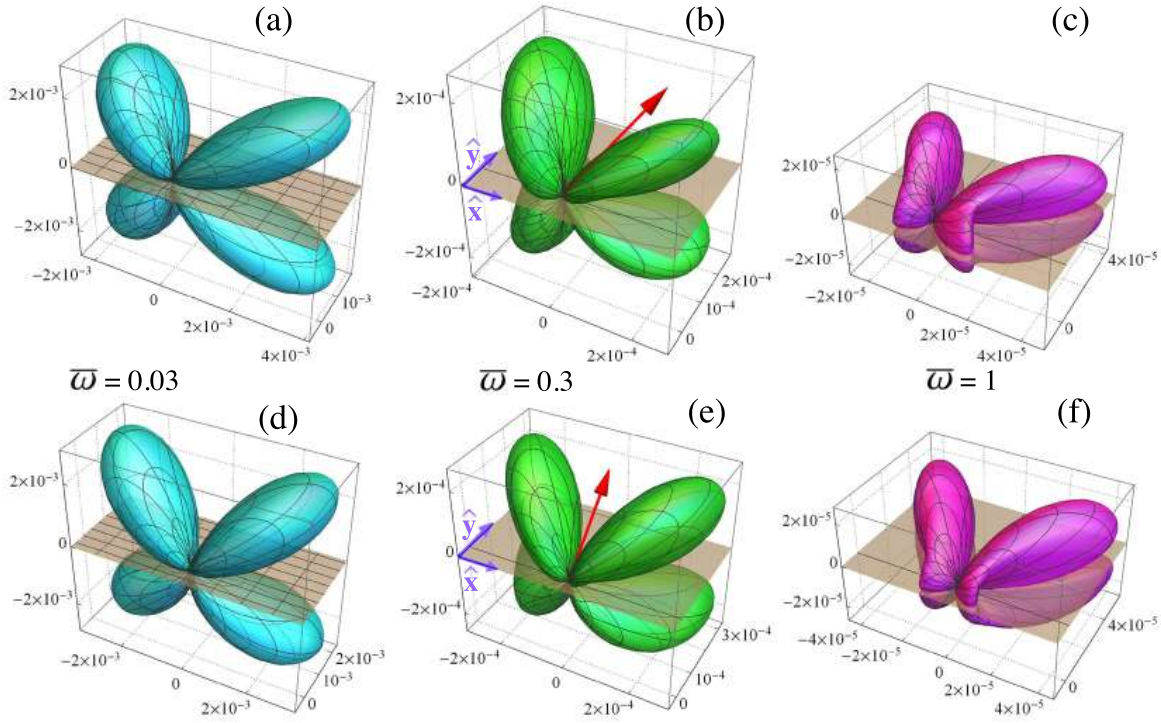


Figure S12: Angular distribution of transition radiation, $\overline{S}(\theta, \phi, \overline{\omega})$, at three reduced frequencies: $\overline{\omega} = 0.03$ (a,d), $\overline{\omega} = 0.3$ (b,e) and $\overline{\omega} = 1$ (c,f) for a charged particle at the reduced speed $\beta = 0.5$ with the oblique incidence angle $\theta_0 = 45°$ upon phosphorene, moving in the in-plane directions defined by $\phi_0 = 45°$ (a,b,c) and $\phi_0 = 90°$ (d,e,f).

Finally, in Fig. S12(a,b,c), we show the TR spectra from phosphorene when the charged particle moves with an in-plane direction of $\phi_0 = 45°$, which is intermediate between the AC and ZZ directions. Comparing them to the spectra for $\phi_0 = 0$ in Fig. S11(a,b,c) and those for $\phi_0 = 90°$ in Fig. S12(d,e,f), one can notice a closer similarity to the latter case, i.e., the spectra in Fig. S12(d,e,f). In a way, one could say that motion in the ZZ direction exerts a stronger "pull" on the TR spectra than the motion in the AC direction. A similar observation could be also made for the TR spectra in Fig. S13, corresponding to a particle moving at the speed $\beta = 0.5$ with the oblique angle $\theta_0 = 75°$ upon phosphorene, in the in-plane direction of $\phi_0 = 45°$, which is intermediate to the in-plane directions displayed in the top ($\phi_0 = 0$) and bottom ($\phi_0 = 90°$) rows

in Fig. 6 of the MT for the same oblique angle. Namely, the TR spectra in Fig. S13 are more similar to those in the bottom row than in the top row in Fig. 6 of the MT.

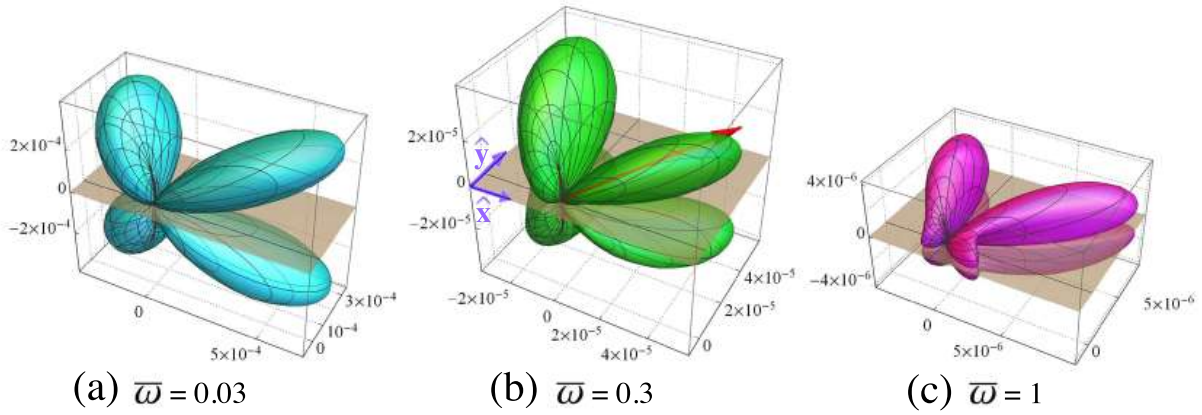


(a) $\overline{\omega} = 0.03$ (b) $\overline{\omega} = 0.3$ (c) $\overline{\omega} = 1$

Figure S13: Angular distribution of transition radiation, $\overline{S}(\theta, \phi, \overline{\omega})$, at three reduced frequencies: $\overline{\omega} = 0.03$ (a), $\overline{\omega} = 0.3$ (b) and $\overline{\omega} = 1$ (c) for a charged particle at the reduced speed $\beta = 0.5$, with the oblique incidence angle $\theta_0 = 75^\circ$ upon phosphorene, moving in the in-plane direction defined by $\phi_0 = 45^\circ$.

# References


(1) Tai, C.; Antennas, I.; Society, P.; Theory, I. M.; Society, T. *Dyadic Green Functions in Electromagnetic Theory*; IEEE Press Series on Electromagnetic Waves; IEEE Press, 1994.

(2) Stratton, J. *Electromagnetic Theory*; An IEEE Press classic reissue; Wiley, 2007.

(3) Miskovic, Z. L.; Segui, S.; Gervasoni, J. L.; Arista, N. R. Energy losses and transition radiation produced by the interaction of charged particles with a graphene sheet. *Physical Review B* **2016**, *94*, 125414.

(4) Miskovic, Z. L.; Akbari, K.; Segui, S.; Gervasoni, J. L.; Arista, N. R. Relativistic effects in the energy loss of a fast charged particle moving parallel to a two-dimensional electron gas. *Nuclear Instruments and Methods in Physics Research Section B: Beam Interactions with Materials and Atoms* **2018**, *422*, 18 – 23.

(5) Akbari, K.; Segui, S.; Mišković, Z. L.; Gervasoni, J. L.; Arista, N. R. Energy losses and transition radiation in graphene traversed by a fast charged particle under oblique incidence. *Phys. Rev. B* **2018**, *98*, 195410.

(6) Akbari, K.; Miskovic, Z. L.; Segui, S.; Gervasoni, J. L.; Arista, N. R. Energy Losses and Transition Radiation in Multilayer Graphene Traversed by a Fast Charged Particle. *ACS Photonics* **2017**, *4*, 1980–1992.

(7) Margulis, V. A.; Muryumin, E. E. Theory for surface polaritons supported by a black-phosphorus monolayer. *Phys. Rev. B* **2018**, *98*, 165305.

(8) Nemilentsau, A.; Low, T.; Hanson, G. Anisotropic 2D Materials for Tunable Hyperbolic Plasmonics. *Phys. Rev. Lett.* **2016**, *116*, 066804.